Two-Dimensional Compact Variational Mode Decomposition-Based Low-Light Image Enhancement

FENGJI MA, JUNYI CHAI, AND HAI WANG, (Member, IEEE)

School of Aerospace Science and Technology, Xidian University, Xi'an 710071, China

Corresponding author: Hai Wang (wanghai@mail.xidian.edu.cn)

ABSTRACT In this paper, a novel methodology is proposed for low-light image enhancement. The proposed algorithm contains three stages: image reconstruction, image enhancement and color restoration. Two-dimensional compact variational mode decomposition (2D-TV-VMD) is employed to covert the RGB image into gray map through decomposing it on multiple gray eigenfunctions. A binary artifact indicator function is used to identify and eliminate potential artifact pixels in an image, and then low-light image enhancement via illumination map estimation (LIME) is used to enhance the reconstructed gray-scale map. Finally, color restoration is performed in RGB-color space to recover the color information. Subjective evaluation and objective evaluation of the proposed method, including no-reference image quality metric of contrast-distorted images based on information maximization (NIQMC), is conducted on different low-light images. Objective and subjective experimental performance demonstrate the competitive performance of the proposed algorithm compared with other state-of-art methods.

INDEX TERMS Two-dimensional compact variational mode decomposition, low-light image enhancement, color restoration, artifact detection.

I. INTRODUCTION

Low-illumination enhancement is an important process to improve the quality of images. One common issue on object detection and tracking is how to display clearly the detail information of low-light images, which might cause severe interference with object recognition. To solve this issue, it is of great need to significantly enhance the illumination of the photos under the premise of preserving the details of the dark area. However, this enhancement process, which is highly non-linear, is very challenging to implement. The key points of the enhancement process lie in estimation of illumination map, color restoration and preservation of detail information. Generally, the enhancement methods fall into four categories: histogram equalization (HE) [1]–[4] based enhancement methods, dehazing model [4] based enhancement methods, Retinex theory [6] based enhancement methods and deep learning based enhancement methods [7]. HE has been extensively employed due to its efficiency and simplicity of

implementation. However, there are several drawbacks in HE such as chromatic aberration and loss of detail information in the enhanced output image. Although dehazing model improves visual quality to some extent, the enhanced image does not always accord with real scenes, since the distortion is incurred by lack of illumination instead of particles in air. Deep learning [7] based enhance-ment methodology averts the parameter adjustment process and makes colors more coordinated. However, the training set involves images with different illumination in the same scene, which is hard to achieve. Retinex method [6] improves image contrast and brightness, in which color information and details are well preserved. However, this method still has its drawbacks like flaring.

Unlike ordinary image enhancement [8], the algorithm for low illumination images are more complicated. Low-light image enhancement via illumination map estimation (LIME) [9] is an enhancement algorithm based on Retinex method. In this algorithm, the illumination of each pixel is first estimated individually by finding the maxi-mum value of the R, G and B channels. The overall structure is preserved

by the fidelity of the initial illumination map and the fine illumination map, and the weighting matrix and gradient are used for keeping the structure smoothness. A generalized Lagrangian function is constructed based on the initial illumination map. The algorithm processes can achieve a re-markable enhancement on the low illumination image at a fast speed, but it has a lackluster performance on image contrast enhancement. Naturalness Preserved En-hancement Algorithm (NPEA) [10] is proposed to preserve natural-ness while enhancing details. This algorithm en-hances natural retention with brightness-order error measurements. The methodology, which decomposes the image into reflectivity and illuminance, adopts a dual logarithmic transformation for the illuminance map to ensure both natural balance and image detail preservation. This methodology can attain good enhancement results and visual effect for low-light pictures, especially in night scenes, but its speed is relatively slow. The variational-based fusion model (VBFM) [11] can achieve both global and local contrast enhancement, and the variation-based fusion model is used to balance the results of them. Contrast limited adaptive histogram equalization (CLAHE) [12] limits the contrast of the image by calculating the local histogram of the image and redistributing the brightness to change the image contrast. A preset threshold is used to copy the histogram to limit the magnified amplitude. The algorithm can improve the local contrast of input image and enhance the details of the image, especially the details of low-light images in dark areas. MultiScale Retinex (MSR) [6] consists of three scales (small, intermediate, and large) that achieve synchronous dynamic range compression/ color consistency/ brightness reproduction. At the same time, a color repair method is defined which produces good color reproduction at the expense of moderate dilution of color consistency. MSR does not achieve great enhance-ment effect, and the disadvantages are obvious that sometimes MSR incurs serious color distortion.

Numerous multiscale signal decomposition methods have been proposed for image enhancement, for instance, wavelet transform [13], empirical mode decomposition (EMD) [5], [14], [15], variational mode decomposition (VMD) [16], etc. The wavelet transform, which has been widely employed, is used to sparsely decompose a given signal at different scales according to selected wavelet basis function and decomposition scale. It captures both frequency information and time or spatial (in terms of a two-dimensional signal) information. The empirical mode decomposition is a self-adaptive decomposition method which recursively decomposes a signal into different modes of separate spectral bands and has been widely used for non-stationary signal analysis. However, due to its lack of mathematical theory and its high dependence on extremal point finding methods, EMD suffers from several obvious limitations such as poor noise or sampling robustness. VMD is a new non-stationary signal processing method. It has been proved to be able to overcome many shortcomings of EMD. It effectively decomposes a signal into different band-limited modes according to

different central frequencies, such that the decomposed modes reproduce the input signal exactly or up to gaussian noise. The decomposed modes, known as intrinsic mode function (IMF), are defined as AM-FM signals [16], [17]. Like EMD, VMD is also an adaptive non-recursive decom-position method and performs well for analysis of both stationary and non-stationary signals. VMD has a solid theoretical background and is more robust to noise and sampling compared with EMD. 2D-VMD [16], [18], [19] expanded the 1D-VMD to two or more dimensions. A two-dimensional analytical signal is introduced to design the 2D decomposition model analogous to the 1D predecessor [20]. The 2D-VMD method has been widely applied in image processing, including image dehazing [5], image denoising [21]–[23], image enhancement [24], object detection [25], etc. 2D-TV-VMD [30] was introduced to take the disconnection of derivatives of input 2D signal into consideration. A binary support function A_k is introduced to describe the sudden signal onset and offset, which does not meet the smoothness of AM-FM modulation. Total variation (TV) and L^1 norm of A_k are utilized to promote spatial sparsity and the resulting optimization problem is solved through ADMM [26].

In this paper, a novel VMD based image enhancement methodology is proposed. First, the conversion from RGB to HSI is conducted on the input color image and the brightness map is taken. 2D-TV-VMD processing is then performed on the extracted map and the reconstructed intensity map is enhanced by LIME method. The Final step is color recovery, which is performed in RGB color space. The proposed algorithm can be applied to process many tricky low-light images. Meanwhile, subjective and objective comparisons with other state-of-the-art algorithms is made to verify the superiority of our algorithms.

Compared with other methods, the conventional Retinex-based low-light image enhancement algorithms achieve relatively good enhancement results. However, these methods suffer from a weakness that they cannot handle the noise pixels and artifacts of images sufficiently. To overcome this drawback, the proposed methodology de-compose and reconstruct the input image utilizing 2D-TV-VMD where the potential noises and artifacts can be adequately eliminated with the L^2 norm and the pre-defined optimization of the threshold. Since many enhancement algorithms suffer from the potential drawback of color distortion, a novel color restoration method is proposed to overcome it. The local similarities of the processed intensity map are used to restore the color as well as to keep the smoothness of the processed image. Such an operation not only preserves the naturalness of the image, but also removes the potential noise and artifact pixels.

In summary, the major contributions of this paper are presented as follows:

1. A novel image enhancement algorithm is proposed based on 2D-TV-VMD model which decomposes the input image into several sub-modes.

2. The proposed method can sufficiently eliminate the artifact and noise pixels due to the introduction of an artifact indicator and the filtering properties of 2D-TV-VMD.

3. A novel color restoration method is proposed to avoid color distortion while keeping the naturalness of output image.

4. The proposed method achieves higher NIQMC values than most existing enhancement algorithms.

The organization of this paper is as follows. Section 2 presents a brief review on 2D-TV-VMD and LIME methods. Section 3 describes the proposed image enhancement methodology in detail. Section 4 demonstrates the experimental results and the evaluations. Finally, con-clusions are given in Section 5.

II. RELATED WORK

A. LIME METHOD

As mentioned above, LIME [9] is a low-light image enhancement method based on Retinex model. Unlike multiscale Retinex (MSR) which treats reflectivity as the ultimate enhanced factor leading to over-enhancement [6], LIME aims to enhance low-light images by estimating its illumination map. The basic enhancement model [6], [27] is formulated as follows:

$$\mathbf{L} = \mathbf{S} \cdot \mathbf{T} \qquad (1)$$

where the base layer $\mathbf{T}$ is a smoothly varying illumination and can be used to constitute an illuminance map. The detail layer $\mathbf{S}$ contains detail and structural information of the image, which is the desired recovery.

LIME decomposes the image into reflectance and illumination components and speeds up the calculation only by estimating the illuminance layer. By slightly transforming (1), we can get $\mathbf{S} = \mathbf{L}/\mathbf{T}$. The estimation of the illuminance map $\mathbf{T}$ is the key to the recovery of the desired enhanced image $\mathbf{S}$. In this way, this problem of how to obtain completely the detail information of low-light images is converted into estimating an illumination map $\mathbf{T}$.

The following formula can be used to handle non-uniform illumination:

$$\hat{T}(\mathbf{X}) \leftarrow \max L(\mathbf{X}) \qquad (2)$$

where $\hat{T}(\mathbf{X})$ represents the initial illumination map. The LIME algorithm first constructs an illumination map by finding the maximum intensity of each pixel in the R, G, and B channels. The lighting structure is then used to refine the lighting map and the augmented Lagrange multiplier method [30] is applied to efficiently solve the refinement problem.

B. 2D-TV-VMD

The 2D-TV-VMD algorithm [16], [18], [19], [29] decomposes an input image f into k discrete modes (sub-signals), where k is assumed to be priori. Each mode has very limited bandwidth around its characteristic central frequency ω_k, and

the fundamental goal of the algorithm is to obtain the modes with specific sparse properties while re-producing the input signal f. The bandwidth of each mode in spectral domain is used to determine its sparsity prior and is estimated through the squared L^2 norm of the gradient, or the H^1 Gaussian smoothness of the demodulated sub-signal. To deal with the spatial compactness of the decomposed modes and capture the sudden onset and offset of the input signal, binary support functions A_k is introduced for conditional constraint. Total variation and L^1 norm of A_k are considered to sufficiently penalize the support area, i.e., to promote spatial compactness or spatial sparsity of each decomposed sub-signal. Unlike 1-D analytical signal which is generally obtained using Hilbert transform, many definitions of n-D analytical signal have been proposed to properly reveal the properties of n-D analytical signal. Inspired by the unilateral-spectrum property of 1-D analytical signal, the n-D Hilbert transform is defined as follows to obtain a two-dimensional analytical signal:

$$\hat{f}_{AS} : \mathbb{R}^n \to \mathbb{C}$$
$$\boldsymbol{\omega} \mapsto \begin{cases} 2\hat{f}(\boldsymbol{\omega}), & \text{if } \langle \boldsymbol{\omega}, \boldsymbol{\omega}_k \rangle > 0 \\ \hat{f}(\boldsymbol{\omega}), & \text{if } \langle \boldsymbol{\omega}, \boldsymbol{\omega}_k \rangle = 0 \\ 0, & \text{if } \langle \boldsymbol{\omega}, \boldsymbol{\omega}_k \rangle < 0 \end{cases} \qquad (3)$$

where the n-D Fourier transform is defined as

$$\hat{f}(\boldsymbol{\omega}) := \mathcal{F}\{f(\cdot)\}(\boldsymbol{\omega}) = (2\pi)^{-n/2} \int_{\mathbb{R}^n} f(\mathbf{x}) e^{-j\langle \boldsymbol{\omega}, \mathbf{x} \rangle} d\mathbf{x} \qquad (4)$$

As mentioned previously, the decomposed sub-modes are first converted to their corresponding analytical signals, which can be easily achieved with (3). Mathematically, the resulting constraint problem can be formulated as:

$$\min_{u_k:\mathbf{R}^n \to \mathbf{R}, A_k:\mathbf{R}^n \to \{0,1\}, \omega_k \in \mathbf{R}^n} \Big\{ \sum_k \alpha_k$$
$$\times \Big\| \nabla \Big[u_{AS,k}(\mathbf{X}) e^{-j<\omega_k, \mathbf{X}>} \Big] \Big\|_2^2$$
$$+ \beta_k \|A_k\|_1 + \gamma_K TV(A_k) \Big\}$$

$$s.t. \ \forall \mathbf{X} \in \mathbf{R}^n : \sum_k A_k(\mathbf{X}) u_k(\mathbf{X}) = f(\mathbf{X}) \qquad (5)$$

C. COLOR RESTORATION

There are two main types of commonly used color image decomposition methods. One is to separately decompose image pixels on the R, G, and B channels. However, this method results in the color information to be highly mixed in the base layer and the detail layer, and the image color is severely distorted. The other is to extract the intensity image by YUV or HSI color conversion, decompose the intensity map, and perform specific operations for the base layer and the detail layer. Despite this method will weaken the color edges and textures, it is much better than the first method. In most cases, the second method is adopted. Color channels
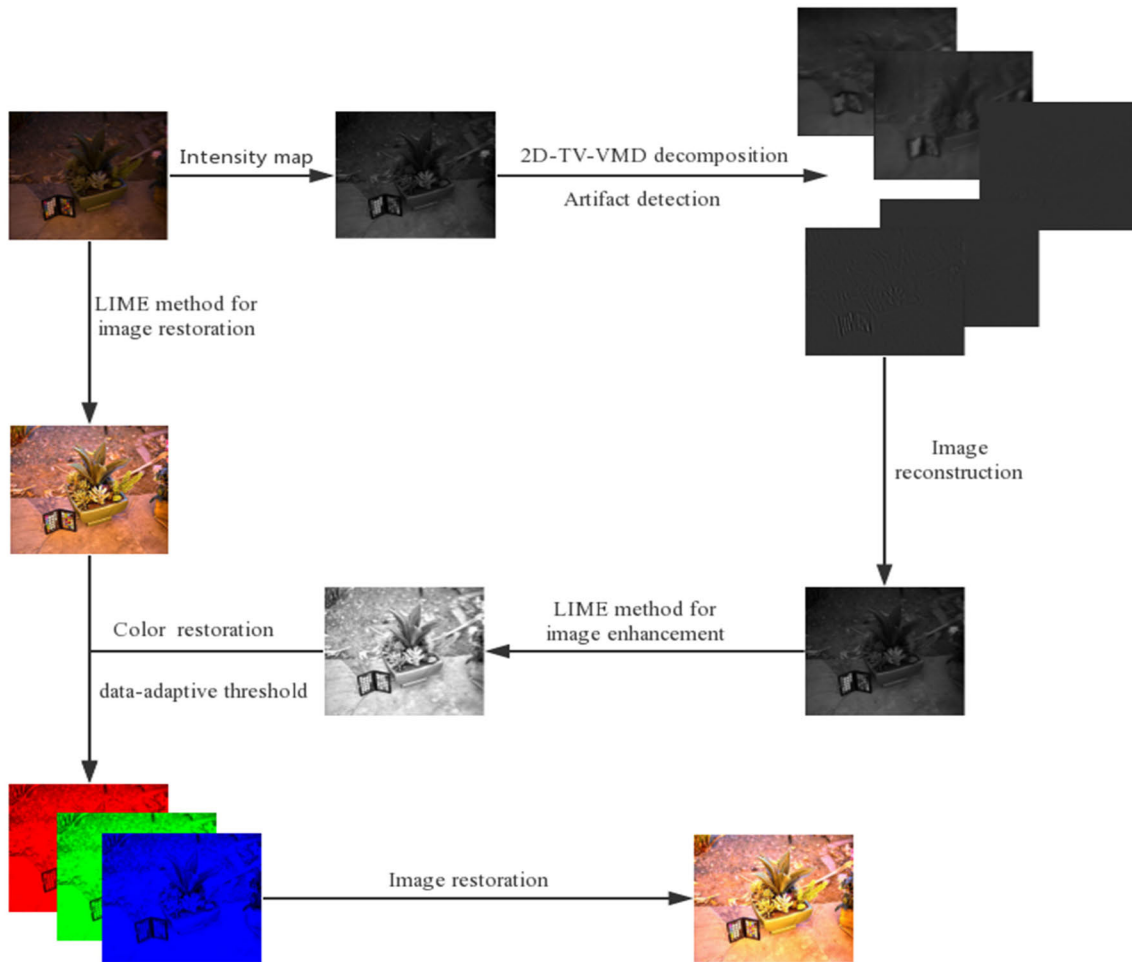
FIGURE 1. Flowchart of the proposed algorithm.

are usually reproduced as follows:

$$\hat{L}_k = (\frac{L_k}{L})^c L_0 \qquad (6)$$

where $L_k, k \in \{R, G, B\}$ is the color channel of the input image, L is the intensity image, and c is the scalar parameter [35].

III. THE PROPOSED 2D-TV-VMD BASED LOW-LIGHT IMAGE ENHANCEMENT METHOD

The proposed method contains three parts. The input image is first decomposed into several sub-modes to detect and remove image artifacts. LIME method is then applied for the low-light map enhancement. The last part is to restore the color information and obtain the enhanced color image. The flowchart of the proposed method is shown in Fig.1

A. IMAGE DECOMPOSITION AND ARTIFACT DETEC-TION

The 2D-TV-VMD algorithm converts the pixel matrix of a color image into the dimension of the HSI space, i.e., the luminance information. To eliminate the potential influence

of artifacts, an artifact indicator function is introduced,

$$\chi : \mathbf{R}^n \rightarrow \{0, 1\} \qquad (7)$$

where $\chi(\mathbf{X}) = 1$ indicates an image artifact at $\mathbf{X}$. Since there do not exist a concise definition about artifact, an artifact is defined as what it fails to achieve, that is, the band-limited properties of the extracted modes. Hence a certain pixel is defined as an artifact where the incurred data-fidelity cost is too large. The new constraint problem can now be modified as

$$\min_{u_k:\mathbf{R}^n \rightarrow \mathbf{R}, A_k:\mathbf{R}^n \rightarrow \{0,1\}, \omega_k \in \mathbf{R}^n} \{\sum_k \alpha_k$$

$$\times \left\| \nabla \left[u_{AS,k}(\mathbf{X}) e^{-j<\omega_k, \mathbf{X}>} \right] \right\|_2^2$$

$$+ \beta_k \|A_k\|_1 + \gamma_K TV(A_k) + \delta \|\chi\|_1\}$$

$$s.t. \, \forall \mathbf{X} \in \mathbf{R}^n : \sum_k (1 - \chi(\mathbf{X})) A_k(\mathbf{X}) u_k(\mathbf{X})$$

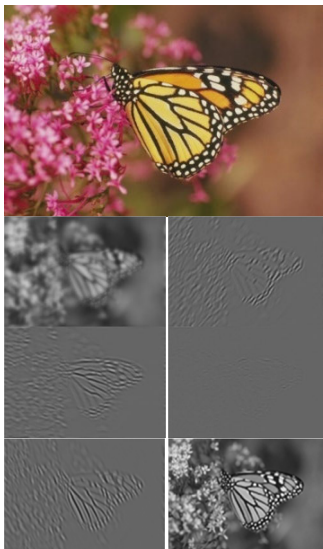$$= (1 - \chi(\mathbf{X})) f(\mathbf{X}) \qquad (8)$$

FIGURE 2. Test image (Monarch butterfly) for 2D-TV-VMD.

FIGURE 3. Two processed low-light pictures after color restoration. The color information of the initial low-light images are well recovered with our restoration method.

where the total variation is defined as

$$TV(A_k) := \sup_{|\phi| \leq 1} < A_k, div\phi >, \quad \text{for } \phi : \mathbf{R}^n \to \mathbf{R}^n$$

The corresponding unconstrained optimization problem is formulated as follows:

$$\ell(\{u_k\}, \{v_k\}, \{A_k\}, \chi, \{\lambda_k\}) :$$
$$= \{\sum_k \alpha_k \left\| \nabla \left[u_{AS,k}(\mathbf{X}) e^{-j<\omega_k, \mathbf{X}>} \right] \right\|_2^2 + \beta_k \|A_k\|_1 + \gamma_K TV(A_k)$$
$$+ \delta \|\chi\|_1 + \rho \left\| (1 - \chi(\mathbf{X}))(f(\mathbf{X}) - \sum A_k(\mathbf{X}) v_k(\mathbf{X}) \right\|_2^2$$
$$+ \sum_k \rho_k \|u_k(\mathbf{X}) - v_k(\mathbf{X})\|_2^2 + < \lambda_k(\mathbf{X}), u_k(\mathbf{X}) - v_k(\mathbf{X}) >\}$$

$$(9)$$

Fig.2 demonstrates the decomposition and reconstruction result of 2D-TV-VMD with artifact detection. The first color picture is the original picture, the last picture in the bottom right is the reconstructed picture after 2D-TV-VMD processing, and the middle five pictures are five modes decomposed by 2D-TV-VMD. The first decomposed mode, which

are often utilized as means of image smoothing or filtering, captures mostly the low-frequency information of the original image and preserves most the detail infor-mation, while the other four decomposed modes captures the high-frequency information, i.e. the edge of the image. Due to the filtering and artifact detecting properties of 2D-TV-VMD, the reconstructed intensity map looks slightly different from the original picture.

B. LOW-LIGHT IMAGE ENHANCEMENT
A color image signal forms a three-dimensional matrix. 2D-TV-VMD merely deals with the luminance information (a two-dimensional matrix) to obtain different mode, which can be formulated as

$$L(\mathbf{X}) = \sum_k (1 - \chi(\mathbf{X})) A_k(\mathbf{X}) u_k(\mathbf{X}) \quad (10)$$

Mathematically, Retinex model can be formulated as a product of the restored image S and the illumination map T.

Based on (1), (7) can be rewritten as

$$S(\mathbf{X}) = \frac{L(\mathbf{X})}{\hat{T}(\mathbf{X}) + \varepsilon} \quad (11)$$

where ε is a very small constant to avoid the appearance of the zero dominator when calculating the recovered image **S** from the illumination map **T**. L^2 norm of the difference of the original illumination map and the estimated illumination map are utilized to keep the overall structure, and L^1 norm of the gradient of estimated illumination map to preserve the smoothness of textural details. The following optimization problem can be depicted as:

$$\min_{\mathbf{T},\mathbf{G}} \{ \left\| \hat{\mathbf{T}} - \mathbf{T} \right\|_2^2 + \alpha \|\mathbf{W} \cdot \mathbf{G}\|_1 \}, \quad s.t. \nabla \mathbf{T} = \mathbf{G} \quad (12)$$

where α is the optimization coefficient which balances L^1 norm and L^2 norm. **W** is the weight matrix, and **G** is an auxiliary variable to replace $\nabla \mathbf{T}$. The augmented Lagrangian equation of the above formula (10) is expressed as

$$\aleph(\mathbf{T}, \mathbf{G}, \mathbf{Z}) = \left\| \hat{\mathbf{T}} - \mathbf{T} \right\|_2^2 + \alpha \|\mathbf{W} \cdot \mathbf{G}\|_1 + \frac{\mu}{2} \|\nabla \mathbf{T} - \mathbf{G}\|_2^2$$
$$+ < \mathbf{Z}, \nabla \mathbf{T} - \mathbf{G} > \quad (13)$$

where **Z** is the Lagrangian multiplier. The restored image **S** is thus given as

$$\mathbf{S} = \frac{\sum_k (1 - \chi(\mathbf{X})) A_k(\mathbf{X}) u_k(\mathbf{X})}{\mathbf{T}} \quad (14)$$

C. COLOR RESTORATION VIA RATIO INFORMATION OF COLOR CHANNELS
When an image contains both severe color distortion and dark appearance, the visual effect of images processed in the RGB space will be better than that in the HSV-color space [30], [31], [37]. The artifacts and noise problems existing in low-light pictures are handled by the 2D-TV-VMD in the luminance space of the image, which reduces the imbalance of the R, G, and B primary colors caused by the
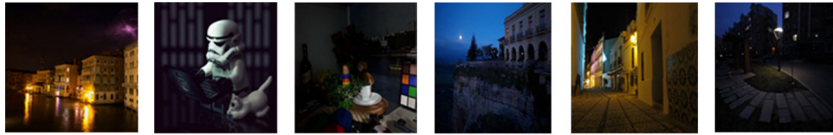
FIGURE 4. Six initial low-light images for compared methods. The images are labeled as follows from left to right: Vennes, Robot, Room, Castle, Street and Community.

RGB spatial processing, resulting in distortion of recovered color image. In order to brighten the dark area of the image as much as possible, in addition to magnifying the brightness value of the image, the pixel values of the R, G, and B channels need to be adjusted separately, and the subsequent image enhancement and color restoration need to be conducted in the RGB space. After simply using the traditional algorithm to perform color recovery on the enhanced intensity map, it is found that the effect is not satisfactory. For our algorithm, we designed a new set of color recovery algorithms. The fundamental idea of the algorithm is to take into account the ratio information between the R, G and B channels, and this ratio is applied to obtain the enhanced color image. To be specific, since the original low-light image might contain potential color distortion, the color restoration algorithm first uses the LIME algorithm to process the original low-light image. The ratio between the channels is extracted from this color image and is applied to the enhanced intensity map to properly restore the color information. The overall color restoration process is formulated as follows:

$$S_0 = \sum_i \eta_i S_i, \quad (i = 1, 2, 3) \quad (15)$$

where S_0 represents the intensity of input image directly processed by LIME. S_1, S_2 and S_3 represent image pixels in the R, G and B channels respectively. The ratio between different channels is given as

$$\lambda_i = \frac{S_i}{S_1}, \quad (i = 1, 2, 3) \quad (16)$$

$$S_i^c = \frac{\lambda_i S^0}{\sum_i \eta_i S_i}, \quad (i = 1, 2, 3) \quad (17)$$

where S^0 represents the intensity of input color image processed with our model. the enhanced image pixels by our algorithm is represented as S_i^c. The restored color image is given as

$$S^c = \Im(S_1^c, S_2^c, S_3^c) \quad (18)$$

where $\Im$ represents a function that converts three two-dimensional matrices into a three-dimensional matrix. To further improve the performance of our restoration methodology, a data-adaptive threshold is introduced to achieve greater image naturalness while removing potential artifacts and noise pixels to enhance lowlight images suffi-ciently. This threshold is used to determine whether a certain pixel should be replaced by the corresponding pixel in images processed

directly through LIME or not. Inspired by [33] and by several window function-based techniques, the data-adaptive threshold is chosen to be based on mean absolute different value of pixels in the current window. To be specific, this pixel-replacement strategy can be formulated as

$$\delta = \frac{1}{N^2} \sum_{(x_n, y_n) \in \Omega_k} \left| S^0(x_n, y_n) - S_0(x_n, y_n) \right| \quad (19)$$

$$S^0(x_n, y_n) = \begin{cases} S^0(x_n, y_n), & \delta > \delta_0 \\ S_0(x_n, y_n), & \delta \leq \delta_0 \end{cases} \quad (20)$$

where Ω_k represents a $N \times N$ window and δ_0 stands for a data-adaptive threshold. Here the threshold is chosen to be 0.05 the average intensity value of pixels by LIME in the window.

D. PROBLEM SOLVING
The core of our model's solution is the algorithm for two saddle point problems. After the luminance map is extracted for the input image, the saddle point problem of the formula (6) is processed by the ADMM [26], and the loops, u_k^t, v_k^t, and ω_k^t are alternately cycled in such a manner that the remaining variables are fixed and the other variables are updated. The binary updated values of χ^* will affect the update of v_k^t and A_k^t, but will not affect the update of u_k^t and ω_k^t. The obtained luminance map is subjected to low-light image enhancement, that is, the above result is calculated by the formula (11), which can be well processed by the ALM [9], [26], [38]. The minimum value problem in equation (10) is coupled with the constraint through a dual variable μ to form an augmented Lagrangian function (11). By optimizing alternately **T, G, Z**, the parameter μ is updated according to the gradient and iterate to the optimal solution. The specific implementation of the proposed methodology is listed in Algorithm 1.

IV. EXPERIMENTS AND RESULTS ANALYSIS
In this section, the performance of our proposed methodology is compared with several state-of-art methods, including MSR, VBFM, LIME, NPEA, guided filter (GF) [34] and rolling guidance filter (RGF) [35]. More than twenty test images are selected and the experiment is implemented in MATLAB with author's support. Fig.4-Fig.5 demonstrates the experimental results and characteristics of each method. VBFM restrains halo effects to some extent at the cost of loss of detail information. Besides, the output images possess relatively good visual effect, and the color information is also preserved well. NPEA highlights details obviously,
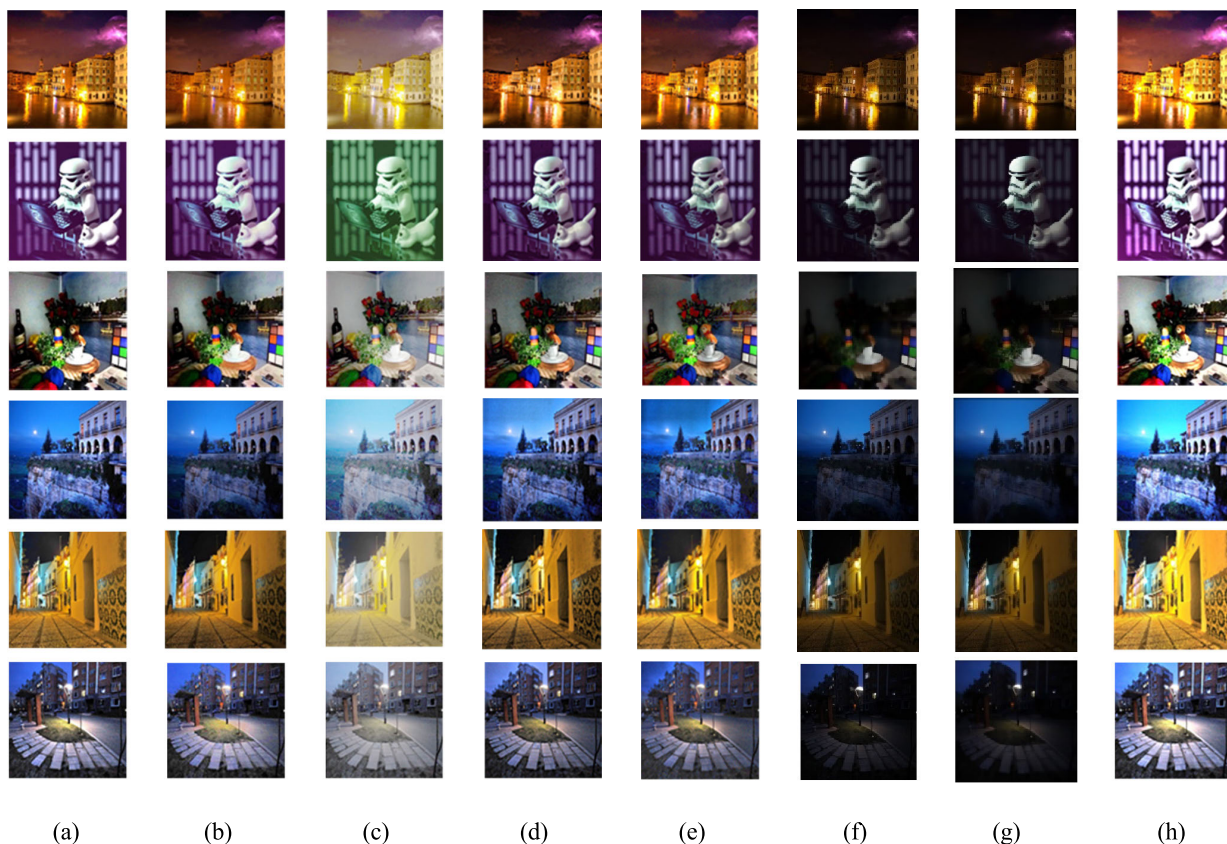
FIGURE 5. Image enhancement results of the compared methods. Figure 5 (a)-(f) are the enhancement results corresponding to six low-illuminance images in Fig. 4 processed by different methods. Figure (a) LIME, (b) NPEA, (c) MSR, (d) VBFM, (e) CLAHE, (f) RGF, (g) GF, (h) Proposed Method.
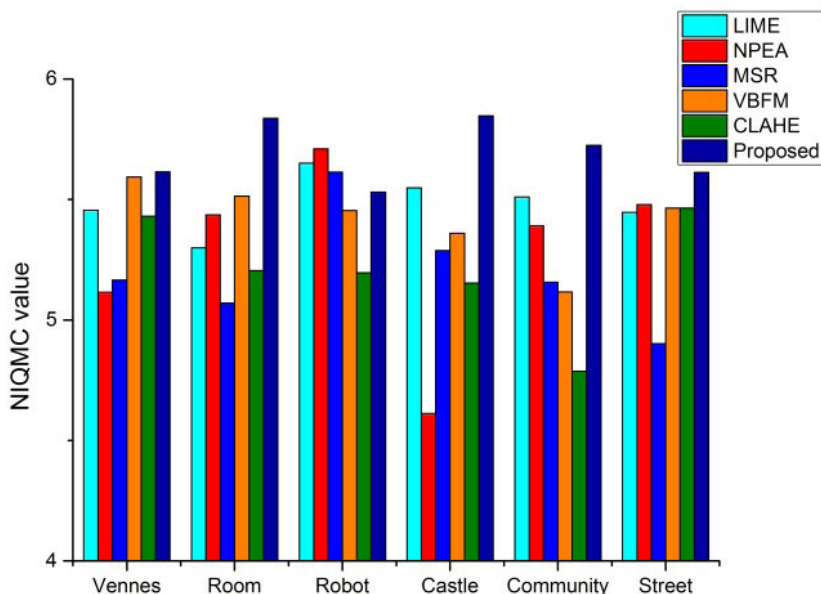
FIGURE 6. NIQMC value test results for compared methods.

but most output images look unnatural due to imbalanced enhancement. Although CLAHE and MSR also preserve the detail information of input images well, the enhanced images lose their original ambience which is important to represent the scene, and the color distortion of output images is severe compared with other enhancement methods. Besides, many

Algorithm 1 2D-TV-VMD Based Low-Light Image Enhancement

Input: signal $f(x)$, number of modes K, parameters α, α_k, β_k, γ_k, ρ, ρ_k, H, τ, τ_k, ϵ, the initial illumination map $\hat{T} \in \mathbb{R}^{m \times n}$.

Output: Optimal solution $T^* = T^{(t)}$.

Initialize $\{\omega_k\}$, $\{u_k^0\} \leftarrow 0$, $\{v_k^0\} \leftarrow 0$, $\{A_k^0\} \leftarrow 1$, $\{\lambda_k^0\} \leftarrow 0$, $\lambda^0 \leftarrow 0$, $n \leftarrow 0$, $T^{(0)} = 0 \in \mathbb{R}^{m \times n}$, $G^{(0)} = Z^{(0)} = 0 \in \mathbb{R}^{2\,m \times n}$, $t = 0$, $\mu^{(0)} > 0$, $\rho_L > 1$

repeat.

$n \leftarrow n + 1$

for $k = 1 \rightarrow K$ **do**

   Create 2 D mask for analytic signal Fourier multiplier:
   $$\mathcal{H}_k^{t+1} \leftarrow 1 + \text{sgn}\left(< \omega_k^t, \omega >\right)$$

   Update $\hat{u}_{AS,k}$:
   $$\hat{u}_{AS,k}^{t+1}(\omega) \leftarrow \mathcal{H}_k^{t+1}(\omega) \left[\frac{\rho_k \hat{v}_k^t(\omega) - \hat{\lambda}_k^t(\omega)}{\rho_k + 2\alpha_k |\omega - \omega^t|^2} \right]$$

   Retrieve u_k:
   $$u_k^{t+1}(x) \leftarrow \mathcal{R}\left(\mathcal{F}^{-1}\left\{ \hat{u}_{AS,k}^{t+1}(\omega) \right\} \right)$$

   Optimal artifact indicator function $\mathcal{X}$:
   $$\mathcal{X}^*(x) \leftarrow \begin{cases} 0 & \text{if} \rho\left(f(x) - \sum A_k(x)v_k(x)\right)^2 \leq \delta \\ 1 & \text{othersise} \end{cases}$$

   if $\mathcal{X}^*(x) = 0$ **then**

      Update v_k:
      $$v_k^{t+1}(x) \leftarrow \frac{\rho A_k^t \left(f(x) - \sum_{i<k} A_i^t(x)v_i^{t+1}(x) - \sum_{i>k} A_i^t(x)v_i^t(x) + \frac{\lambda^t(x)}{\rho} \right) + \rho_k v_k^{t+1}(x) + \lambda_k^t(x)}{\rho A_k^t(x)^2 + \rho_k}$$

      Update A_k through moditied MBO:
      $$A_k^{t+\frac{1}{3}}(x) \leftarrow$$
      $$\frac{A_k^t(x) + H\left(-\beta_k + 2\rho v_k^{t+1}(x)\left(f(x) - \sum_{i<k} A_i^{t+1}(x)v_i^{t+1}(x) - \sum_{i>k} A_i^t(x)v_i^t(x)\frac{\lambda^t(x)}{\rho}\right)\right)}{1 + 2H\rho\left(v_k^{t+1}(x)\right)^2}$$

      $$\hat{A}_k^{t+\frac{2}{3}}(w) \leftarrow \frac{\hat{A}_k^{t+1}(w)}{1 + H\gamma_k|\omega|^2}$$

      $$A_k^{t+1}(x) \leftarrow \begin{cases} 0 & \text{if} A_k^{t+\frac{1}{3}}(x) \leq \frac{1}{2} \\ 1 & \text{if} A_k^{t+\frac{1}{3}}(x) > \frac{1}{2} \end{cases}$$

   else

      Update v_k
      $$v_k^{t+1}(x) \leftarrow u_k(x) + \frac{\lambda_k(x)}{\rho_k}$$

      Update A_k through modifide MBO:
      $$A_k^{t+\frac{1}{3}}(x) \leftarrow \frac{A_k^t(x) + H\left(-\beta_k + 2\rho\left(1 - \mathcal{X}^*(x)^2 v_k^{t+1}(x)\right)\left(f(x) - \sum_{i<k} A_i^{t+1}(x)v_i^{t+1}(x) + \frac{\lambda^t(x)}{\rho(1-\mathcal{X}^*(x))^2}\right)\right)}{1 + 2T\rho\left(1 - \mathcal{X}^*(x)\right)^2 \left(v_k^{t+1}(x)\right)^2}$$

      $$A_k^{t+\frac{2}{3}}(w) \leftarrow \frac{\hat{A}_k^{t+1}(w)}{1 + H\gamma_k|\omega|^2}$$

      $$A_k^{t+1}(x) \leftarrow \begin{cases} 0 & \text{if} A_k^{t+3}(x) \leq \frac{1}{2} \\ 1 & \text{if} A_k^{t+\frac{2}{3}}(x) > \frac{1}{2} \end{cases}$$

   end if

   Update ω_k:
   $$\omega_k^{t+1} \leftarrow \frac{\int_{\mathbb{R}^2} \omega \left| \hat{u}_{AS,k}^{t+1}(\omega) \right|^2 d\omega}{\int_{\mathbb{R}^2} \left| \hat{u}_{AS,k}^{t+1}(\omega) \right|^2 d\omega}$$

   Dual ascent u-v cacpling:
   $$\lambda_k^{t+1}(x) \leftarrow \lambda_k^t(x) + \tau_k \left(u_k^{t+1}(x) - v_k^{t+1}(x) \right)$$

end for

Algorithm 1 *(Continued.)* 2D-TV-VMD Based Low-Light Image Enhancement

Dual ascent data fidelity:
$$\lambda_k^{t+1}(\boldsymbol{x}) \leftarrow \lambda_k^t(\boldsymbol{x}) + \boldsymbol{\tau}\left(f(\boldsymbol{x}) - \sum_k A_k^{t+1}(\boldsymbol{x})v_k^{t+1}(\boldsymbol{x})\right)$$

until convergence

while not converged **do**

Update $\boldsymbol{T}^{(j+1)}$:
$$\boldsymbol{T}^{(j+1)} \leftarrow \mathcal{F}^{-1}\left(\frac{\mathcal{F}\left(2\boldsymbol{T}+\mu^{(j)}\boldsymbol{D}^T\left(\boldsymbol{G}-\frac{\boldsymbol{Z}^{(j)}}{\mu^{(j)}}\right)\right)}{2+\mu^{(j)}\sum_{d\in[h,v]}\overline{\mathcal{F}(\boldsymbol{D}_d)}]\mathcal{F}(\boldsymbol{D}_d)}\right)$$

Update $\boldsymbol{G}^{(j+1)}$
$$\boldsymbol{G}^{(j+1)} \leftarrow S_{\frac{\alpha W}{\mu^{(j)}}}\left[\nabla\boldsymbol{T}^{(j+1)} + \frac{\boldsymbol{Z}^{(j)}}{\mu^{(j)}}\right]$$

Update $\boldsymbol{Z}^{(j+1)}$ and $\mu^{(j+1)}$:
$$\boldsymbol{Z}^{(j+1)} \leftarrow \boldsymbol{Z}^{(j)} + \mu^{(j)}\left(\nabla\boldsymbol{T}^{(j+1)} - \boldsymbol{G}^{(j+1)}\right)$$
$$\mu^{(j+1)} \leftarrow \mu^{(j)}\rho_L, \rho_L > 1$$

$j = j + 1$

end while

TABLE 1. NIQMC value [8] for different methods.

	LIME	NPEA	MSR	VBFM	CLAHE	RGF	GF	Proposed
Vennes	5.4552	5.1148	5.1652	5.5938	5.4302	4.6540	4.6356	**5.6146**
Room	5.2996	5.4357	5.0706	5.5135	5.2051	4.0027	4.0672	**5.8372**
Robot	5.6509	**5.7097**	5.6138	5.4536	5.1956	4.3862	4.4241	5.5310
Castle	5.5488	4.6120	5.2880	5.3594	5.1527	3.8825	3.7719	**5.8472**
Community	5.5102	5.3915	5.1570	5.1165	4.7878	2.7910	2.6311	**5.7249**
Street	5.4465	5.4793	4.9022	**5.7047**	5.4641	4.7722	4.7906	5.6126
Average	5.4852	5.2905	5.1994	5.4569	5.2059	4.0814	4.0534	**5.6945**

real-scene low-light images hide intensive noises in the dark area. After performing LIME, the details of the scene get enhanced, but the noises also come out, which is far from satisfactory for practical usage. This is an inevitable problem encountered by almost all the existing low-light enhancement algorithms. The structure of images processed with RGF and GF are well preserved due to the edge-preserving properties of the two algorithms. However, these two algorithms also loss much detail information of the input images and the overall low-light environments are not sufficiently enhanced, which results in some relatively low NIQMC values. Comparatively, the proposed algorithm achieves a good balance between the detail enhancement and the structure preservation, and the output NIQMC values also demonstrate the algorithm's effective-ness. Besides, due to the noise-filtering and artifact-detecting properties of 2D-TV-VMD, the amount of noise and halo can be greatly reduced.

A. OBJECTIVE ASSESSMENT

Considering that there is no 'true' image in low-light enhancement, the widely adopted no-reference image quality metric for contrast distortion (NIQMC) [36] is considered to quantitatively evaluate the performance of aforementioned algorithms. To clearly address the difference of NIQMC scores between these methods, the histogram is drawn in Fig.6, while Table.1 shows the evaluate results of NIQMC and the highest NIQMC value is highlighted in bold. Our proposed method achieves four of the highest value out of the six test images, indicating the effectiveness of our method.

Fig. 7 shows the average NIQMC value of six different images in our experiments for compare. The proposed method achieves 5.6971, which is the highest NIQMC value among all the compared methods and outperforms the other methods like LIME and NPEA obviously.

B. SUBJECTIVE ASSESSMENT

A subjective evaluation [27], [32] is introduced in addition to objective NIQMC evaluation. To further evaluate the proposed image enhancement method, we adopted the subjective evaluation [33], which is conducted in an indoor room with stable illuminations. In this test, the enhancement results of 15 low-light images processed with aforementioned six enhancement methods are shown and 20 volunteers are
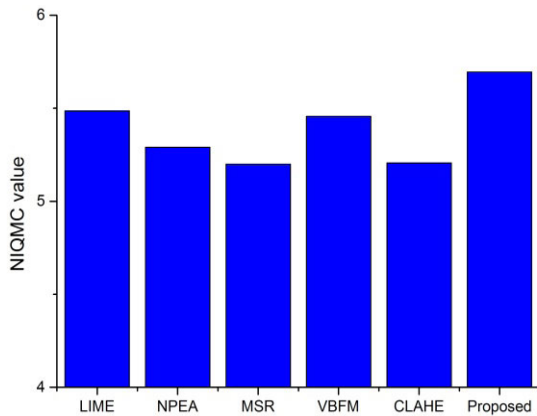
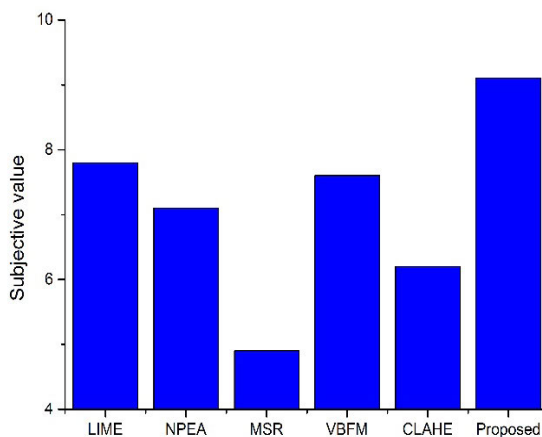**FIGURE 7.** Average NIQMC value test results for compared methods.

FIGURE 8. Subjective results for compared methods.

invited to give rate for each enhanced image with a score from 1 to 10. The mean rating of each method is shown in Fig.8. It is obvious that LIME, VBFM and the proposed method achieve better average rating value and our method achieve 9.1, which is the highest of all tested methods. Besides, MSR and CLAHE achieve relatively low scores, which agrees with the previous analysis.

It is shown clearly from the objective and subjective results that the proposed method achieves good results from the perspective of both low-light enhancement and contrast enhancement in comparison with other state-of-the-art algorithms. Besides, the subjective assessment reveals the good color-restoration property of the proposed method, which benefits much from the modified restoration methodology. However, the proposed method also suffers from some drawbacks like algorithm complexity, and the proposed algorithm does not always achieve better enhancement results. Yet, from a global view, the proposed method still demonstrates its superiority over other methods.

V. CONCLUSION

In this paper, a 2D-TV-VMD based methodology has been proposed for low-illumination color image enhance-ment,

which processes the input image while sufficiently removing artifact and noise pixels. We employed 2D-TV-VMD algorithm to decompose and reconstruct the input image, which converts color map to intensity map and removes halo and noise from the input image. The reconstructed image was then processed with the low-light enhancement method. A modified color restoration method was applied to turn the enhanced intensity map to color map. The experiments demonstrated the advance of our proposed methodology in comparison with other state-of-the-art algorithms. The proposed low-light image enhancement technology can satisfy many vision-based applications such as edge detection, feature matching, object recognition and tracking, with high visibility outputs to improve their performance.

REFERENCES

[1] C. Y. Wong, C. Jiang, M. A. Rahman, S. Liu, S. C.-F. Liu, N. Kwok, H. Shi, Y.-H. Yu, and T. Wu, "Histogram equalization and optimal profile compression based approach for color image enhancement," *J. Vis. Commun. Image Represent.*, vol. 38, pp. 802–813, Jul. 2016.

[2] J. R. Tang and N. A. M. Isa, "Bi-histogram equalization using modified histogram bins," *Appl. Soft Comput.*, vol. 55, pp. 31–43, Jun. 2017.

[3] K. Singh, D. K. Vishwakarma, G. S. Walia, and R. Kapoor, "Contrast enhancement via texture region based histogram equalization," *J. Modern Opt.*, vol. 63, no. 15, pp. 1444–1450, Mar. 2016.

[4] X. Wang and L. Chen, "Contrast enhancement using feature-preserving bi-histogram equalization," *Signal, Image Video Process.*, vol. 12, no. 4, pp. 685–692, May 2018.

[5] H. T. Suseelan, V. Sowmya, and K. P. Soman, "Image dehazing using variational mode decomposition," in *Proc. Int. Conf. Wireless Commun., Signal Process. Netw. (WiSPNET)*, Mar. 2017, pp. 200–205.

[6] D. J. Jobson, Z. Rahman, and G. A. Woodell, "A multiscale retinex for bridging the gap between color images and the human observation of scenes," *IEEE Trans. Image Process.*, vol. 6, no. 7, pp. 965–976, Jul. 1997.

[7] Y. P. Loh, X. Liang, and C. S. Chan, "Low-light image enhancement using Gaussian Process for features retrieval," *Signal Process., Image Commun.*, vol. 74, pp. 175–190, May 2019.

[8] S. Rahman, M. M. Rahman, M. Abdullah-Al-Wadud, G. D. Al-Quaderi, and M. Shoyaib, "An adaptive gamma correction for image enhancement," *EURASIP J. Image Video Process.*, vol. 2016, no. 1, Oct. 2016, Art. no. 35.

[9] X. Guo, Y. Li, and H. Ling, "LIME: Low-light image enhancement via illumination map estimation," *IEEE Trans. Image Process.*, vol. 26, no. 2, pp. 982–993, Feb. 2017.

[10] S. Wang, J. Zheng, H.-M. Hu, and B. Li, "Naturalness preserved enhancement algorithm for non-uniform illumination images," *IEEE Trans. Image Process.*, vol. 22, no. 9, pp. 3538–3548, Sep. 2013.

[11] Q.-C. Tian and L. D. Cohen, "A variational-based fusion model for non-uniform illumination image enhancement via contrast optimization and color correction," *Signal Process.*, vol. 153, pp. 210–220, Dec. 2018.

[12] K. Zuiderveld, *Contrast Limited Adaptive Histogram Equalization Graphics Gems Iv*. New York, NY, USA: Academic, 1994, pp. 474–485.

[13] K. Sui and H. G. Kim, "Research on application of multimedia image processing technology based on wavelet transform," *EURASIP J. Image Video Process.*, vol. 2019, no. 1, Jan. 2019, Art. no. 24.

[14] N. E. Huang, Z. Shen, S. R. Long, M. C. Wu, H. H. Shih, Q. Zheng, N.-C. Yen, C. C. Tung, and H. H. Liu, "The empirical mode decomposition and the Hilbert spectrum for nonlinear and non-stationary time series analysis," *Proc. Roy. Soc. London Ser. A, Math., Phys. Eng. Sci.*, vol. 454, no. 1971, pp. 903–995, Mar. 1998.

[15] S. Mallik, S. S. Khan, and U. C. Pati, "Visual enhancement of underwater image by white-balanced EMD," in *Proc. 8th Int. Conf. Comput., Commun. Netw. Technol. (ICCCNT)*, Jul. 2017, pp. 1–6.

[16] K. Dragomiretskiy and D. Zosso, "Variational mode decomposition," *IEEE Trans. signal Process.*, vol. 62, no. 3, pp. 531–544, Feb. 2014.

[17] J. R. Carson, "Notes on the theory of modulation," *Proc. Inst. Radio Eng.*, vol. 10, no. 1, pp. 57–64, Feb. 1922.

[18] Y. Jiang, Z. Li, C. Zhang, C. Hu, and Z. Peng, "On the bi-dimensional variational decomposition applied to nonstationary vibration signals for rolling bearing crack detection in coal cutters," *Meas. Sci. Technol.*, vol. 27, no. 6, May 2016, Art. no. 065103.

[19] K. Dragomiretskiy and D. Zosso, "Two-dimensional variational mode decomposition," in *Energy Minimization Methods in Computer Vision and Pattern Recognition*. Cham, Switzerland: Springer, 2015, pp. 197–208.

[20] Y. L. Ekinci, S. Özyalin, P. Sindirgi, Ç. Balkaya, and G. Göktürkler, "Amplitude inversion of the 2D analytic signal of magnetic anomalies through the differential evolution algorithm," *J. Geophys. Eng.*, vol. 14, no. 6, pp. 1492–1508, Dec. 2017.

[21] S. Lahmiri and M. Boukadoum, "Biomedical image denoising using variational mode decomposition," in *Proc. IEEE Biomed. Circuits Syst. Conf. (BioCAS)*, Oct. 2014, pp. 340–343.

[22] Q. Xiao, J. Li, and Z. Zeng, "A denoising scheme for DSPI phase based on improved variational mode decomposition," *Mech. Syst. Signal Process.*, vol. 110, pp. 28–41, Sep. 2018.

[23] S. Yu and J. Ma, "Complex variational mode decomposition for slop-preserving denoising," *IEEE Trans. Geosci. Remote Sens.*, vol. 56, no. 1, pp. 586–597, Jan. 2018.

[24] L. M. Satapathy, R. K. Tripathy, and P. Das, "A combination of variational mode decomposition and histogram equalization for image enhancement," *Nat. Acad. Sci. Lett.*, vol. 42, no. 4, pp. 333–336, Aug. 2019.

[25] X. Wang, Z. Peng, P. Zhang, and Y. He, "Infrared small target detection via nonnegativity-constrained variational mode decomposition," *IEEE Geosci. Remote Sens. Lett.*, vol. 14, no. 10, pp. 1700–1704, Oct. 2017.

[26] M. R. Hestenes, "Multiplier and gradient methods," *J. Optim. Theory Appl.*, vol. 4, no. 5, pp. 303–320, 1969.

[27] H. Yue, J. Yang, X. Sun, F. Wu, and C. Hou, "Contrast enhancement based on intrinsic image decomposition," *IEEE Trans. Image Process.*, vol. 26, no. 8, pp. 3981–3994, Aug. 2017.

[28] C. S. Brenner and L. R. Scott, *The Mathematical Theory of Finite Element Methods*. 2008.

[29] D. Zosso, K. Dragomiretskiy, A. L. Bertozzi, and P. S. Weiss, "Two-dimensional compact variational mode decomposition," *J. Math. Imag. Vis.*, vol. 58, no. 2, pp. 294–320, Jun. 2017.

[30] X. Fu, Y. Liao, D. Zeng, Y. Huang, X. Zhang, and X. Ding, "A probabilistic method for image enhancement with simultaneous illumination and reflectance estimation," *IEEE Trans. Image Process.*, vol. 24, no. 12, pp. 4965–4977, Dec. 2015.

[31] D. Wu, B. Han, J. Ning, and W. Ren, "Image enhancement based on contourlet transform," *Proc. SPIE*, vol. 11052, Jan. 2019, Art. no. 1105217.

[32] X. Jia, X. Feng, W. Wang, and L. Zhang, "An extended variational image decomposition model for color image enhancement," *Neurocomputing*, vol. 322, pp. 216–228, Dec. 2018.

[33] Y. Wu, B. Jiang, and N. Lu, "A descriptor system approach for estimation of incipient faults with application to high-speed railway traction devices," *IEEE Trans. Syst., Man, Cybern. Syst.*, vol. 49, no. 10, pp. 2108–2118, Oct. 2019, doi: 10.1109/TSMC.2017.2757264.

[34] K. He, J. Sun, and X. Tang, "Guided image filter," *IEEE Trans. Pattern Anal. Mach. Intell.*, vol. 35, no. 6, pp. 1397–1409, Jun. 2012.

[35] Q. Zhang, X. Shen, L. Xu, and J. Jia, "Rolling guidance filter," in *Proc. Eur. Conf. Comput. Vis.* Cham, Switzerland: Springer, 2014, pp. 815–830.

[36] K. Gu, W. Lin, G. Zhai, X. Yang, W. Zhang, and C. W. Chen, "No-reference quality metric of contrast-distorted images based on information maximization," *IEEE Trans. Cybern.*, vol. 47, no. 12, pp. 4559–4565, Dec. 2017.

[37] F. Luo, B. Du, L. Zhang, L. Zhang, and D. Tao, "Feature learning using spatial-spectral Hypergraph discriminant analysis for hyperspectral image," *IEEE Trans. Cybern.*, vol. 49, no. 7, pp. 2406–2419, Jul. 2019.

[38] L. Zhang, L. Zhang, B. Du, J. You, and D. Tao, "Hyperspectral image unsupervised classification by robust manifold matrix factorization," *Inf. Sci.*, vol. 485, pp. 154–169, Jun. 2019.

FENGJI MA was born in Hebei, China, in 1998. He is currently pursuing the bachelor's degree in aerospace engineering with Xidian University. His research interests include image processing, deep learning, and pattern recognition.
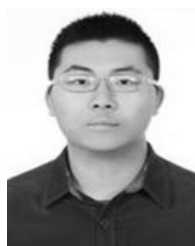
JUNYI CHAI was born in Henan, China, in 1998. He is currently pursuing the bachelor's degree in aerospace engineering with Xidian University. His research interests include image processing and pattern recognition.
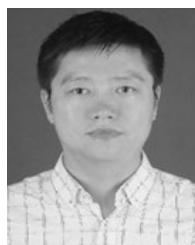
HAI WANG was born in December 1976. He received the B.E. degree in communication engineering, the M.E. degree in communication and information systems, and the Ph.D. degree in measurement and instrumentation from Xidian University, Xi'an, China, in 1998, 2003, and 2007, respectively, where he is currently a Professor. His main research interests include instrumentation and measurements.

● ● ●